Ion Pairing and Hydration in Polyelectrolyte Multilayer Films Containing Polysaccharides

Thomas Crouzier and Catherine Picart*,†

Université de Montpellier 2, CNRS UMR 5539, Place Eugène Bataillon, 34095 Montpellier Cedex 5, France

Received October 29, 2008; Revised Manuscript Received November 25, 2008

Thin films constituted of poly(L-lysine) (PLL) as polycation and of the anionic polysaccharides hyaluronan (HA), chondroitin sulfate (CSA), and heparin (HEP) as polyanions with increasing sulfate contents have been investigated for their internal structure, including water content and ion pairing. Film buildup in physiological solutions was followed in situ by quartz crystal balance with dissipation monitoring (QCM-D) and attenuated total internal reflectance (ATR-FTIR), infrared spectroscopy (ATR-FTIR), which allows an unambiguous quantification of the groups (sulfate, carboxylate, ammonium) present on the side groups of the polyelectrolytes. HA- and CSA-based films were the most hydrated ones. The monomer ratio (disaccharide/lysine) was very similar for all the films, whatever the polyanion, and tended toward a plateau value at ~0.5, indicating that there are two lysine molecules per disaccharide monomer. Thanks to the possibility to selectively cross-link carboxylate and ammonium ions via carbodiimide chemistry, the COO^-/NH_3^+ and SO_3^-/NH_3^+ ion pairing was determined. We found that 46% of NH_3^+ groups are unpaired (i.e., extrinsically compensated by counterions) in HA-based films, 21% in CSA-based films and none in HEP ones, which is indeed in agreement with fluorescence recovery after photobleaching (FRAP) measurements of fluorescently labeled PLL diffusion in the films. In addition, the ratio of SO_3^- versus COO^- pairing with NH_3^+ groups was close to the stoechiometry of these groups in the dissacharide monomeric unit, that is, 2:1 for HEP-based films and 1:1 for CSA based films. Thus, hydration, ion pairing, and PLL diffusion in the films are interconnected properties that arise from the specific structures of the biomacromolecules constituting the films.

Introduction

The internal structure and growth properties of polyelectrolyte multilayers (PEM) are an intensive field of research since the past decade.[1−3] Differences in growth modes, that is, linear versus exponential, have been evidenced depending on the buildup conditions and on the polyelectrolyte intrinsic properties.[4,5] An important question that remains debated is how the charge balance in the films is achieved. In a pioneering work by Schlenoff,[6] the concept of intrinsic, (i.e., polyelectrolyte of opposite charge) versus extrinsic (i.e., counterions) charge matching was introduced. Since then, studies have mostly focused on the widely investigated synthetic polyelectrolyte system PAH/PSS[7] that is mainly found to be "intrinsically" compensated, but few is known about the internal charge balance in films made of natural polyelectrolytes.[8] During past years, an increasing interest has emerged for the investigation of natural-based films[9] due to the fact that these natural polyelectrolytes possess specific properties (enzyme biodegradability, biocompatibility, bioactivity,...) and that they are already widely employed in the biomedical field and in the food sector under various conditioning (gels, capsules, membranes,...).[10] Also and importantly, polyanions like polysaccharides (hyaluronan, chondroitin sulfate, heparan sulfate, and heparin), also called glycosaminoglycans, are natural components of the extracellular matrices (ECM) of soft tissues where they associate with proteins via covalent but also electrostatic interactions.[11] They play a role in the release of growth factors[12] and in the control of tissue hydration.[13] This motivates their use in the design of tissue engineered constructs.[14,15] Self-assembly of natural biopolymers thus gives the possibility to mimic the organization of tissues and to controllably prepare thin reservoirs for bioactive molecules, such as growth factors, to guide cell proliferation and differentiation[16] or to deliver locally drugs such as antitumoral agents.[17]

Here, we chose three important anionic polysaccharides, hyaluronan, chondroitin sulfate A, and heparin with similar structures and chain flexibility (persistence length of the order of 4.5−6 nm[18]) but different charged groups and densities (COO^- and SO_3^- as negative charges) to investigate the influence of these lateral charged groups on film growth, hydration, and ion pairing.

Hyaluronan is a linear polysaccharide constituted of alternated *N*-acetyl-β-D-glucosamine and β-D-glucuronic acid residues (Figure 1A). Hyaluronan possesses lubricating functions in the cartilage and participates in the control of tissue hydration, water transport, and in the inflammatory response after a trauma.[19] It is employed for soft tissue augmentation, articular therapy, and viscosupplementation.[19] Chondroitin sulfate belongs to the glycosaminoglycan family and is an alternating copolymer of *N*-acetyl-β-D-galactosamine and β-D-glucuronic acid that can be sulfated at C4 or C6 (Figure 1B). It is an important structural component of all connective tissues and is a key component of skin,[20] cartilage matrix, and interphotoreceptor matrix.[21] It is also being used in the treatment of the symptoms of arthritis.[22]

Heparin has the highest negative charge density of any known biological molecule and contains one carboxylic group and several sulfate groups.[23] The most common disaccharide unit is composed of a 2-O-sulfated iduronic acid and 6-O-sulfated,

* To whom correspondence should be addressed. E-mail: catherine.picart@minatec.grenoble-inp.fr.
† Present address: Minatec-PHELMA LMGP, 3 parvis Louis Néel, 38016 Grenoble Cedex.

10.1021/bm8012378 CCC: $40.75
Published on Web 01/13/2009

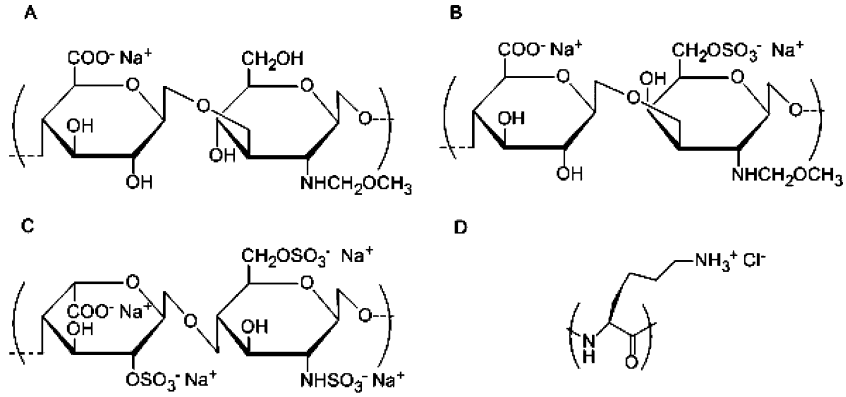

Figure 1. Chemical structures of the four polyelectrolytes used in this study. The three polyanions with carboxylic and sulfate negative charges are (A) hyaluronan, (B) chondroitin sulfate A, and (C) heparin. The polycation employed is poly(L-lysine) (D).

N-sulfated glucosamine (Figure 1C). Heparin is mainly used as anticoagulant in solution or adsorbed onto surfaces,[24] but it is also known to specifically interact with numerous growth factors that control cell fate.[25] For this reason, it is widely studied for its interactions with proteins[23] and is also structurally mimicked for designing cell targets.[26] All these polysaccharides have already been widely used in a variety of biomedical applications, including tissue engineering,[27−29] controlled drug release, and capsule formation.[30]

Interestingly, disaccharide monomer units can be considered as natural building blocks with tuneable charge, HA being the less charged (one COO^- group, no sulfate group), CSA being intermediate with a COO^-/SO_3^- stoechiometry of 1:1, and HEP being the more charged and sulfated one with a mean stochiometry of 1:2.5 (the HEP dissacharides bearing either two or three sulfate groups, a mean value is usually taken).[31] Beside electrostatic interactions, also commonly called "salt bridges", interactions of the disaccharide monomer units with the solvent molecules (usually water containing salt like NaCl or KCl for a physiological medium) via hydrogen bonds are of prime importance for determining their structure, hydration properties, and interactions with oppositely charged molecules.[32] Hydrogen bonds were indeed found to be very important in the buildup of homopolynucleotide films.[33] Both carboxylate and sulfate groups are known to drive essential biological interactions between glycosaminoglycans and proteins that mediate cell adhesion processes, growth factor storage and delivery in the ECM.[11]

The polypeptide poly(L-lysine) (Figure 1D) was chosen as a simple model representing the more complex proteins such as Myrisotylated Alanine-rich C kinase substrate that interact via their lysine and arginine residues with the glycosaminoglycans in the natural ECM.[34] In addition, PLL has already been widely employed as a polycationic component in LbL films.

In this study, our aim was to study the influence of the COO^- and SO_3^- groups on (i) film growth, (ii) water content (film hydration), and (iii) ion pairing in these natural-based films. We have used FTIR-ATR to obtain information on the internal chemical structure of the films as well as on ion pairing, as this technique is now a well-established technique to quantitatively investigate the internal structure of PEM films[2,35] and allows each individual charged group to be followed. In particular, the use of a cross-linking protocol specific to carboxylic groups will allow us to determine the respective percentage of NH_3^+ groups interacting with COO^- versus SO_3^- groups. Quartz crystal microbalance with dissipation monitoring was employed to obtain information on the hydration of the deposited layers.

Experimental Section

Polyelectrolyte Solutions. Anionic hyaluronan solutions (HA, 200 kDa, Medipol, Lausanne, Switzerland, molecular weight (MW) of the monomeric unit 378 g/mol), chondroitin sulfate A (CSA, 75 kDa, Sigma, Saint-Quentin Fallavier, France, MW of the monomeric unit 457 g/mol), and heparin solution (HEP, H4784, 15 kDa Sigma, Saint-Quentin Fallavier, France, MW of the monomeric unit 494 g/mol) were dissolved at 1 mg/mL in a buffered Hepes-NaCl solution (20 mM Hepes, 0.15 M NaCl, pH 7.4) in water for the QCM-D experiments or in 0.15 M NaCl in D_2O adjusted at pH 7.4 for the FTIR experiments. HA is a polyanionic macromolecule (one carboxylic group /disaccharide unit) with a $pK_a \sim 2.9$. The pK_a of CSA (one carboxylic group and one sulfate group/disaccharide unit) is even lower due to the presence of the sulfate ($pK_{asulfate} = 2-2.5$) group.[36] HEP (one carboxylic group and 2 to 3 sulfate groups per disaccharide unit) is a strong polyelectrolyte.[31] Given the pK_a of the basic and acidic groups present in the polymers, full ionization of the polyelectrolytes was achieved at pH 7.4, as confirmed by the infrared analysis of COO^- and COOH peaks of the polyelectrolytes and of the polyelectrolyte multilayer films. Poly(L-lysine) hydrobromide (PLL, Sigma, P2636, MW 68 kDa) was prepared at 0.5 mg/mL in the same solutions. During film buildup, all the rinsing steps were performed with the salt containing solution and films were never dried.

Films Characterization by Quartz Crystal Microbalance with Dissipation Monitoring (QCM-D). The $(PLL/PolyA)_8$ film buildup (PolyA for polyanions and films containing eight layer pairs) was followed by in situ quartz crystal microbalance (QCM-Dissipation, Qsense, Sweden).[37] The quartz crystal was excited at its fundamental frequency (about 5 MHz, $\nu = 1$) as well as at the third, fifth, and seventh overtones ($\nu = 3$, 5, and 7 corresponding to 15, 25, and 35 MHz, respectively). Changes in the resonance frequencies Δf and in the relaxation of the vibration once the excitation is stopped were measured at the four frequencies.

When a thin and rigid film of mass Δm is adsorbed at the crystal and the measurements are conducted in air, the resulting decrease Δf typically obeys the Sauerbrey equation:[38]

$$\Delta m = -C\Delta f/n \tag{1}$$

where C is the mass sensitivity constant (17.7 ng·cm^{-2} Hz^{-1} at 5 MHz), and n is the overtone number.

For a viscoelastic film, the QCM-D response has been modeled using a Voigt based model,[39] (i.e., a spring and dashpot in parallel under no slip conditions). It is assumed that the film is homogeneous, with a uniform thickness. The frequency changes (Δf) and the dissipation factor changes (ΔD) can thus be written

$$\Delta f \approx -\frac{1}{2\pi\rho_0 h_0}\left\{\frac{\eta_C}{\delta_C} + t\rho_F\omega - 2t\left(\frac{\eta_C}{\delta_C}\right)^2 \frac{\eta_F\omega^2}{\mu_F^2 + \omega^2\eta_F^2}\right\} \tag{2}$$

and

$$\Delta D \approx -\frac{1}{\pi f \rho_0 h_0}\left\{\frac{\eta_C}{\delta_C} + 2t\left(\frac{\eta_C}{\delta_C}\right)^2 \frac{\eta_F \omega^2}{\mu_F^2 + \omega^2 \eta_F^2}\right\} \quad (3)$$

where ω is the angular frequency of the oscillation and ρ_0 and h_0 are the density and thickness of the crystal, respectively. The viscosity of the bulk liquid is η_C, $\delta_C = (2\eta_C/\rho_C\omega)^{1/2}$) is the viscous penetration depth of the shear wave in the bulk liquid and ρ_C is the liquid's density. The thickness, density, viscosity, and elastic shear modulus of the adsorbed layer are represented by t, ρ_F, η_F, and μ_F, respectively.

By assuming the density and viscosity of the bulk liquid (ρ_C, η_C are 1000 kg·m^{-3} and 1 mPa·s, respectively, and a fixed density of the layer (ρ_F = 1009 kg·m^{-3}), the *Qtools* software (Qsense, Gotenborg, Sweden) estimates the thickness, viscosity, and shear modulus of the adsorbed layer. The fundamental frequency was always disregarded for this analysis.

Film Characterization and Cross-Linking by FTIR. The (PLL/PolyA)$_8$ film buildup on a ZnSe crystal and its subsequent cross-linking were investigated by in situ Fourier transform infrared (FTIR) spectroscopy in attenuated total reflection (ATR) mode with a Vertex 70 spectrophotometer (Bruker Optic Gmbh, Ettlingen, Germany). All the experimental details have been given previously.[40,41] The experiments were performed in a deuterated 0.15 M NaCl solution at pH 7.4. D_2O is used as the solvent instead of water because the amine band of PLL and HA and the carboxylic band of HA and CSA are affected by the strong water band absorption around 1643 cm^{-1} (O−H bending), whereas the corresponding vibration in D_2O is found around 1209 cm^{-1}. During the buildup, the film was continuously in contact with the 0.15 M NaCl solution and was never dried. After each polyelectrolyte deposition (4 mL for each layer were flushed in the measuring cell), rinsing step, and the final contact with the cross-linking solution, single-channel spectra from 64 interferograms were recorded between 400 and 4000 cm^{-1} with a 2 cm^{-1} resolution, using Blackman-Harris three-term apodization and the standard Bruker OPUS/IR software (version 6.5). The spectrum from the bare ZnSe crystal in contact with the 0.15 M NaCl solution (pH 7.4) was taken as reference.

For film cross-linking, 2 mL of 1-ethyl-3-(3-dimethylaminopropyl)-carbodiimide hydrochloride (EDC) and 2 mL of *N*-hydroxysulfosuccinimide (sNHS) were dissolved in a solution of 0.15 M NaCl (in D_20) at pH 5.5 (adjusted by adding of few droplets 0.1 M HCl in D_20), mixed v/v, and subsequently flushed in the measuring cell. Cross-linking was allowed to proceed for 12 h. The parameters and configuration used for the acquisition during the cross-linking reaction have already been given in detail.[41] Spectra were acquired before and after cross-linking.

Peak Assignment and Quantification by FTIR. For a quantitative analysis of the adsorbed amounts and internal structure of the films, spectra of the polyelectrolyte solutions in contact with the non adsorbing crystal were first performed. For HA, the carboxylic peaks at 1610 cm^{-1} and 1414 cm^{-1}, an amide band in the 1635 cm^{-1} region, as well as characteristic peaks of saccharide rings in the 950−1100 cm^{-1} region were observed (Figure 2A).[41] For CSA, observed were carboxylic peaks at 1606 cm^{-1} and 1412 cm^{-1}, the amide I band at 1635 cm^{-1}, and a strong vibration shows up at 1063 cm^{-1} corresponding to the sulfated group[42] (Figure 2B). In the heparin spectrum, the carboxylic peak at 1610 cm^{-1} and the sulfate group at 1000 cm^{-1} were the most intense peaks (Figure 2C), this latter peak was attributed to the antisymmetric vibrations of C−O−S groups.[43]

The amide band of PLL is visible in the 1670−1630 cm^{-1} region, with two peaks at 1635 cm^{-1} and 1670 cm^{-1} (Figure 2D) tentatively attributed to random and turn structures, respectively.[44] Usually, the bands between 1700 and 1525 cm^{-1} composed of both carboxylic (around 1610 cm^{-1}) and amide I (mainly at 1640 and 1670 cm^{-1}) bands needed to be deconvoluted after residual water removal and baseline correction. This was achieved by means of the Opus Software (Bruker, Germany). The most consistent results were obtained when the amide band was assumed to be Gaussian and the COO^- assumed to be 70% Lorenzian and 30% Gaussian.

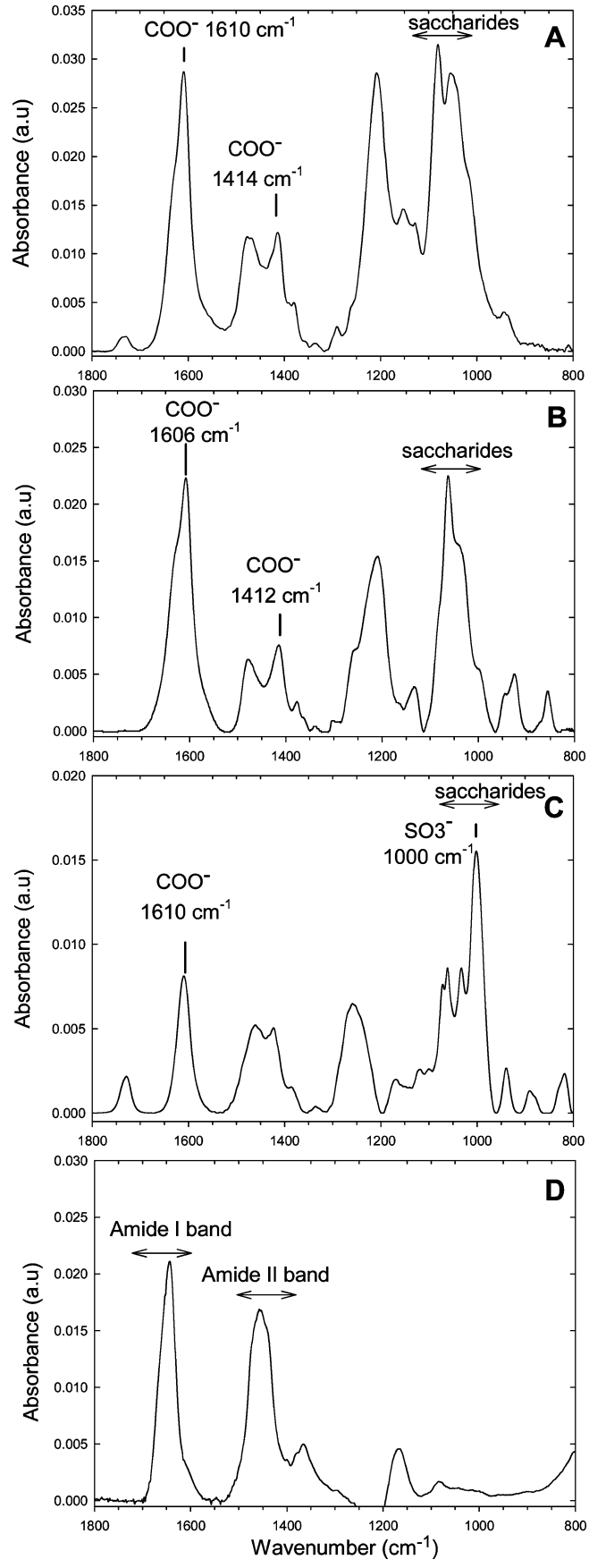

Figure 2. FTIR calibration spectra and major peak assignments. FTIR spectra of HA at 15 mg/mL (A), CSA at 15 mg/mL (B), HEP at 10 mg/mL (C), and PLL at 15 mg/mL (D) are shown with the peaks used for quantification.

Table 1. Nature of the Chemical Bond, Corresponding Wavenumber, Penetration Depth, and Calibration Factor[a]

chemical bond	wavenumber (cm^{-1})	d_P (nm)	K abs/(mg/mL)
PLL C=O (amide I)	1635	962.04	4.66×10^{-3}
PLL C=O (amide I)	1670	941.88	7.1×10^{-4}
HA COO^-	1610	976.98	1.8×10^{-3}
CSA COO^-	1606	979.42	1.15×10^{-3}
Hep C−O−S	1000	1572.94	1.52×10^{-3}

[a] Calculated from the calibration curves (see Figure S1).

Calibration curves allowed us to determine that about 70% of the PLL dissolved in a D_2O solution had an amide band at 1635 cm^{-1} and 30% at 1670 cm^{-1}. These two peaks and their ratio were also verified when PLL was adsorbed at each deposition step during the polysaccharide film buildup, for all three polysaccharides. As hyaluronan also contains an amide band adsorbing in the same region, the maximum peak intensity could not be directly taken for quantification. Thus, the increase in amide I band intensity after each PLL deposition was summed and used to calculate the total PLL amount.

For the quantification, the knowledge of the penetration depth of the evanescent wave, d_p,[45] and of the calibration constant K given below are required:

$$d_P = \frac{\lambda}{2\pi n_1 \left[\sin^2(\theta) - \left(\frac{n_2}{n_1}\right)\right]^2} \quad (4)$$

with λ representing the wavelength of the incident light, n_1 and n_2 are the refractive indices of the ZnSe and medium, respectively (2.42 and 1.34), and θ is the incident angle (45°).

In the case of an infinite medium, the absorbance can be derived:[45]

$$A = KC \quad \text{with} \quad K = \frac{n_2}{n_1}\frac{\varepsilon}{\cos\theta}\frac{d_P}{2} \quad (5)$$

The calibration constant K was determined for specific peaks. For this, polyelectrolyte solutions of known concentrations were brought into contact either with a nonadsorbing bare ZnSe crystal as previously described.[2,46] The carboxylic peak was chosen for the quantification of HA and CSA, the sulfate peak for HEP and the amide I band for PLL (Table 1). From the slope of the absorbance for a given band, the constants were obtained for the various polyelectrolytes (Figure SI1 and Table 1). We assumed that the calibration curve could be extrapolated to higher absorbance values as those measured during film buildup, since such high values could not be obtained using polyelectrolyte non adsorbing solutions. For quantitative analysis of the films, the analysis was always performed on films after buffer rinsing to get solely the contribution of adsorbed polymer molecules that remained irreversibly bound to the crystal surface. The expression of the absorbance of an adsorbed film with a finite thickness t, can be derived from optical equations given by Harrick.[47]

$$A = K\frac{n'_2}{n_2}\rho_F\left(1 - \exp\left(-2\frac{t}{d_P}\right)\right) = K\frac{n'_2}{n_2}\rho_F F(t/d_P) \quad (6)$$

where n'_2 is the refractive index of the film (taken to be 1.38 for HA and CSA films[48] and 1.55 for HEP films[49]). The knowledge of $F(t/d_p)$ is required. In our experiments, the penetration depth of the evanescent wave was large (~1 μm) relative to the thickness of the multilayers (of the order of 100 nm at most) and $F(t/d_p)$ is increasing only weakly with t/d_p. Thus, a linear approximation for the $F(t,d_p)$ function was used with a slope of 1.81 (see Figure SI2). In our conditions, using, $\Gamma = \rho_F xt$ this leads to:

$$\Gamma = \frac{d_P}{1.81K}\frac{n_2}{n'_2}A \quad (7)$$

The adsorbed amount Γ can thus be easily deduced from the measured A, known K, and calculated d_p.

Charge Matching. For quantitative determination of the charge matching, covalent cross-linking of amine and carboxylic groups was achieved by means of an established protocol,[50] making use of the water-soluble carbodiimide EDC in the presence of sNHS. When this protocol was used, only COO^- and NH_3^+ group react together. For each type of film, films were cross-linked to their maximum using an EDC concentration of 150 mg/mL. Then, a second cross-linking (at EDC 100 mg/mL) was performed to check whether the film was already cross-linked to its maximum. No change in FTIR spectra could be noticed after the second cross-linking, meaning maximum cross-linking was achieved successfully after the first cross-linking. We also hypothesize that only NH_3^+ and COO^- groups in close vicinity will be cross-linked and transformed into an amide bond. The total carboxylic content was determined by assuming the presence of one COO^- group per HA, CSA, and HEP monomer (Figure 1). In a first step, the decrease in COO^- groups after cross-linking was quantified. Then, based on the fact that one COO^- group interacts with one NH_3^+ group, the percentage of COO^- groups interacting with NH_3^+ groups could be deduced. Finally, by knowing the total NH_3^+ group content (one NH_3^+ per PLL monomer), the percentage of NH_3^+ groups interacting with COO^- groups could be determined. In sulfated polymers, the same strategy was applied and we hypothesized that NH_3^+ groups would interact preferentially with sulfate groups than with counterions, as both SO_3^- and NH_3^+ are weakly hydrated ions (chaotrope), whereas Na^+ is a strongly hydrated ion (kosmotrope).[51,52] By determining the total sulfate group content (one SO_3^- per CSA monomer and 2.5 per HEP monomer), we determined -NH_3^+/SO_3^- and NH_3^+/Cl^- pairing.

Fluorescence Recovery after Photobleaching (FRAP). FRAP experiments were performed using the LSM 510 confocal microscope (Carl Zeiss, Germany) with a 25 mW Argon laser as previously described.[53] The films were photobleached over a ~60 μm circular region with the laser at 25% laser power and time-lapse microscopy was subsequently performed by acquiring the images every 2 min over a 30 min period. The images were analyzed using the LSM software. As the exact determination of the diffusion coefficient requires a complex simulation procedure, we used a simplified form of this equation (see Supporting Information).

Results and Discussion

Film Buildup, Hydration, and PLL Diffusion. The buildup of the three types of films was followed by QCM-D at four different resonance frequencies (5, 15, 25, and 35 MHz; Figure 3). The highest decrease in frequencies was recorded for $(PLL/HA)_8$ films followed by $(PLL/CSA)_8$ films. The lowest changes were observed for $(PLL/HEP)_8$ films. Of note, for both (PLL/CSA) and (PLL/HEP), the reduced frequencies perfectly overlap, indicating rather rigid layers. These films are characterized by a linear relationship between mass and frequency shift. In contrary, PLL/HA films exhibit a viscoelastic behavior that can not be described by the Sauerbrey model.[3] Film thickness and adsorbed masses deduced from the Voinova model are given in Figure 4 and Table 2, respectively. Of note, similar results were obtained for CSA and HEP-based films by applying the Sauerbrey equation (data not shown). The $(PLL/HA)_8$ film thickness reached ~430 nm, $(PLL/CSA)_8$ films reached ~300 nm, and $(PLL/HEP)_8$ films were the thinnest at ~80 nm. The adsorbed amounts followed the same trend with 45.8, 25.0, and 6.4 $\mu g/cm^2$, respectively, for HA, CSA, and HEP-based films (Table 2). Film thickness grows exponentially as a function of the number of layers for PLL/CSA films similarly to HA, in agreement with a previous study on PLL/CSA films.[21] On the other hand, PLL/HEP films grow rather linearly and much less than the other films, which is in accordance with a previous optical waveguide lightmode spectroscopy studies on the same system.[49] In contrast, when HEP is associated in LbL films with

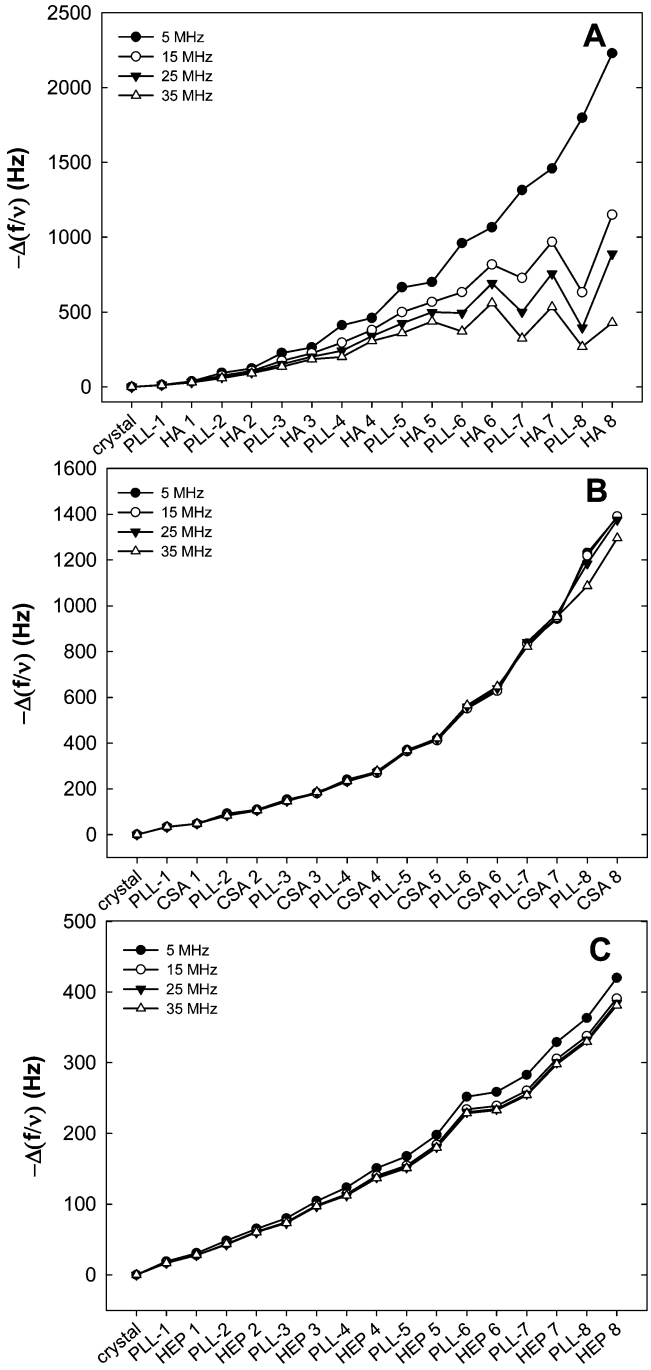

Figure 3. Film growth followed by in situ QCM-D. Differences in the frequency shifts ($\Delta f/\nu$) measured at the end of each polycation and polyanion deposition for (A) PLL/HA, (B) PLL/CSA, and (C) PLL/HEP.

a synthetic and hydrolytically degradable polycation, film growth was found to be of exponential type and HEP was thought to diffuse within the film.[54]

It is now acknowledged that the solvent molecules contribute to QCM-D signal,[55] whereas infrared spectroscopy measures the film dried mass. Thus, comparison between QCM-D and FTIR data can give useful information on film dry mass and hydration.[8] FTIR spectra were thus acquired for the films built in situ on the ATR crystal.

An increase of specific bands was noticeable after each polyelectrolyte deposition (Figure 5). In (PLL/HA) films, this was particularly visible for amine I and saccharide bands as well as for the COO^- group at 1610 cm^{-1} (Figure 5A). For

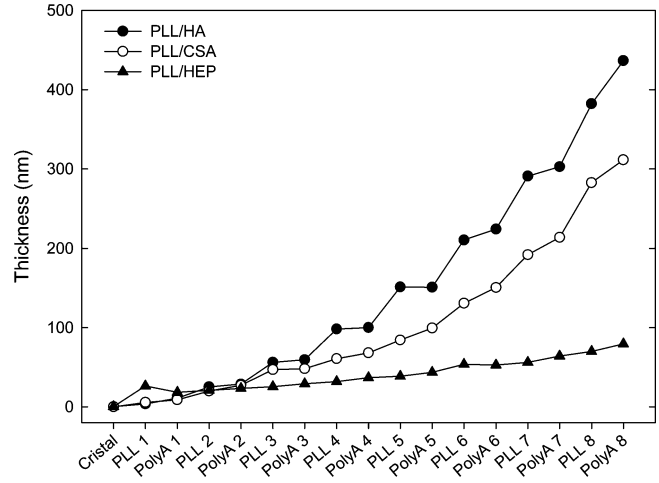

Figure 4. Film thickness as a function of the number of layer pairs deduced from the QCM-D data (same experimental conditions as in Figure 3) for PLL/HA (●) PLL/CSA (○), and PLL/HEP (▲) films. PolyA stands for each polyanion deposition for all three types of films.

Table 2. Adsorbed Masses Determined from the ATR-FTIR and QCM-D Data for PLL and PolyA[a]

	mass	PLL $\mu g/cm^2$	PolyA $\mu g/cm^2$	total mass $\mu g/cm^2$	hydration (% w/w)
PLL/HA	FTIR	5.2	5.6	10.8 ± 2.7	76%
	QCM	41.3	4.5	45.8 ± 17	
PLL/CSA	FTIR	3.5	5.8	9.3 ± 1.7	63%
	QCM	15.5	9.5	25.0 ± 0.6	
PLL/Hep	FTIR	2	3.1	5.1 ± 0.6	20%
	QCM	2.2	4.2	6.4 ± 2.2	

[a] Film hydration is calculated from the ratio of total masses (mean of three independent experiments).

PLL/CSA films, a similar pattern emerged, but with an additional SO_3^- peak showing up at 1063 cm^{-1} (Figure 5B). For (PLL/HEP) films, deposition of PLL increased the amide I band (1635 cm^{-1}), whereas deposition of HEP led to an increase in the COO^- peak (1610 cm^{-1}) and SO_3^- peak (1000 cm^{-1}, Figure 5C). From each individual spectrum and from the known calibration constants (Table 1), the adsorbed amounts of each polyanion and polycation were calculated for each deposited layer (Figure 6). In consistency with QCM-D data, growth curves were exponential for HA and CSA-based films and deviate only slightly from linearity for the HEP films. The growths are also in accordance with the QCM-D data, with the highest adsorbed amounts for HA and the lowest for HEP-based films. However, the adsorbed amounts calculated from FTIR data were systematically smaller than those estimated from the QCM-D measurements. Comparison between FTIR and QCM data allows film hydration to be estimated (Table 2). The thickest (PLL/HA) and (PLL/CSA) films are the most hydrated ones (respectively, ~76 and ~63%), while (PLL/HEP) are only weakly hydrated (~20%). It has to be noted that the reproducibility of the experiments was in the range of 5 to 15%, depending on the type of film (three independent experiments for each type of film).

In thick films exhibiting exponential growth, one expects PLL to diffuse as already shown for (PLL/HA) films.[5] We thus measured the diffusion coefficient of PLL in the three types of films by FRAP experiments (Figure 7). PLL in PLL/HA films has the highest mean diffusion coefficient (~0.064 $\mu m^2/s$), followed by PLL in PLL/CSA films (~0.044 $\mu m^2/s$). As expected, PLL in HEP films is barely or not diffusing at all (~0.00348 $\mu m^2/s$), that is, 20-fold less that in HA-based films.

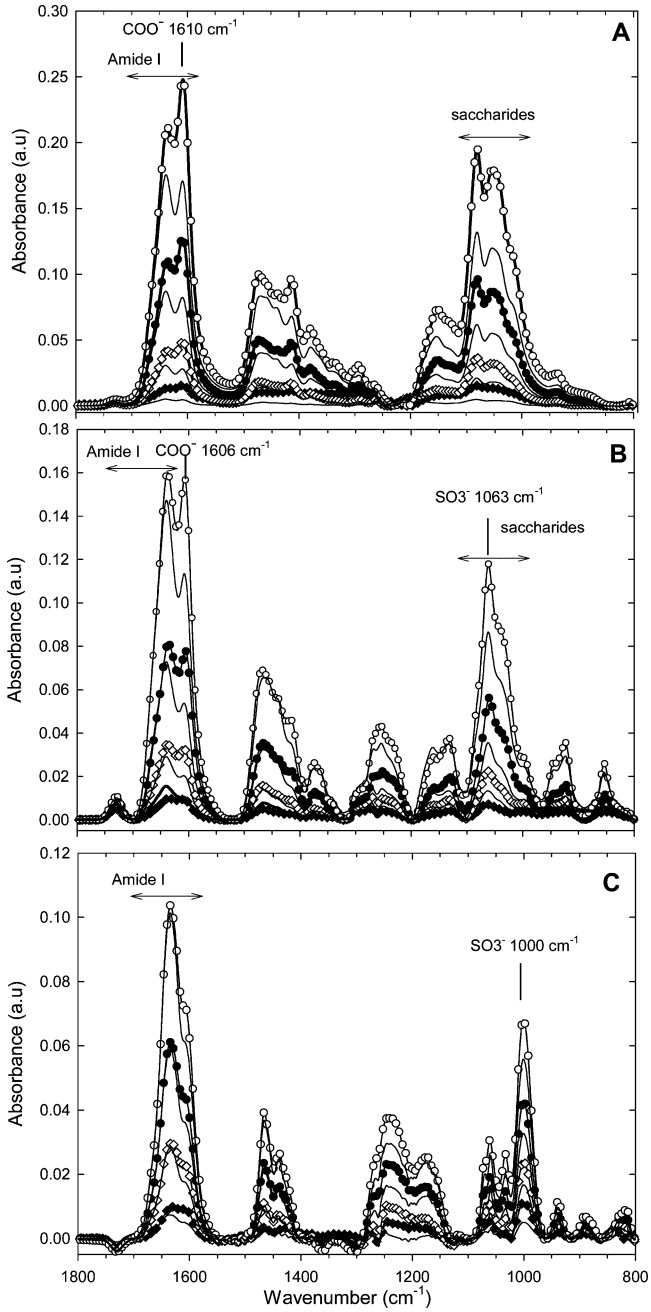

Figure 5. FTIR spectra acquired during the buildup of multilayer films. For clarity, only absorbance spectra of the polyanion layers after deposition of a pair number of layers are shown, 2 (◆), 4 (◇), 6 (●), and 8 (○), (A) for $(PLL/HA)_8$ films, (B) for $(PLL/CSA)_8$ films, and (C) for $(PLL/HEP)_8$ films. Polycation deposited layers are all represented as thin lines.

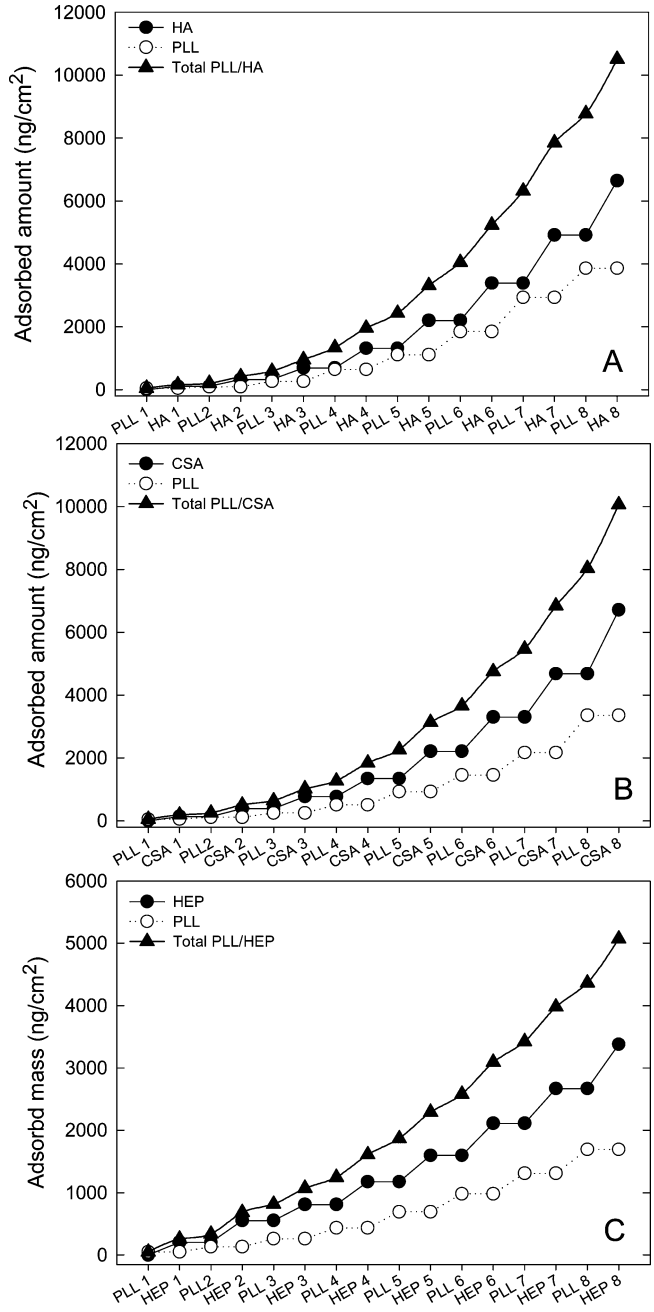

Figure 6. Calculated polyelectrolyte adsorbed amounts from the FTIR individual spectra acquired after each layer deposition. For each type of film, the PolyA (●), PLL (○), and the total PLL/PolyA (▲) adsorbed amounts are represented: (A) (PLL/HA), (B) (PLL/CSA), and (C) (PLL/HEP).

Such values for diffusion of PLL in PLL/HA films are in accordance with diffusion measurements previously performed by confocal FRAP method[53] and by the fluorescence recovery after pattern photobleaching method.[56]

Quantitative Analysis of the Disaccharide Monomer/Lysine Ratio and of the Charge Ratio. FTIR not only allows the adsorbed amounts to be calculated but also to get better insight into the internal chemical structure of the films. In particular, the ratio of polyanion over polycation monomers can be calculated at each deposition step (Figure 8). This ratio oscillates and tends to stabilize around 0.5 after the deposition of five layer pairs. It was systematically slightly higher when the polyanion layer was deposited. Very interestingly, the oscillation pattern and ratio values are very similar for the three types of films whatever the nature of the polyanion. This indicates that, although the absolute charges of the disaccharide units are very different, the overall ratio of disaccharide unit to lysine monomer is constant and does not depend on the polysaccharide monomer charge. Thus, all the films contain about two lysine monomers per disaccharide unit. This may be due to steric hindrance, the PLL monomer length being ~ 0.38 nm,[57] whereas the disaccharide units length are of the order of 1 nm (~1.01 nm for HA[19] and 0.913 nm for CSA).[58] For PLL/HEP films, one may have hypothesized that more than two monomers would interact with the HEP disaccharide, as it bears ~3.5 negative charges. These similarities might be due to the similar structures of the polyanions (disaccharide units). Thus,

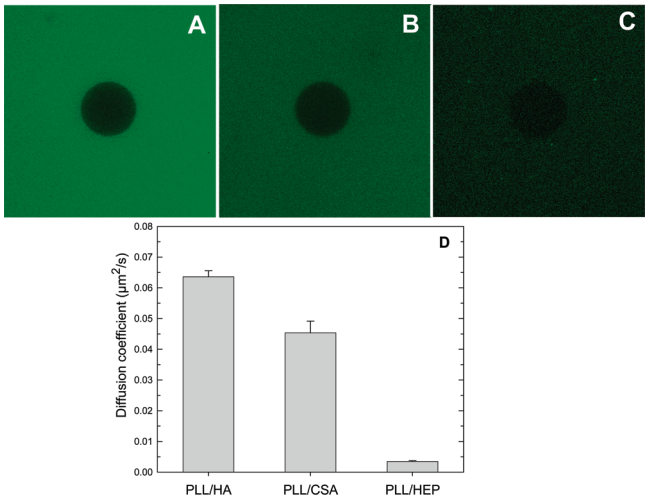

Figure 7. Representative images of FRAP experiments for (A) PLL/HA, (B), PLL/CSA, and (C) PLL/HEP films taken with a confocal laser scanning microscope immediately after the bleach. The diameter of the bleached circular area is 58.7 μm. (D) Mean diffusion coefficients ($\pm$ standard deviation) averaged from four independent measurements on four different samples.

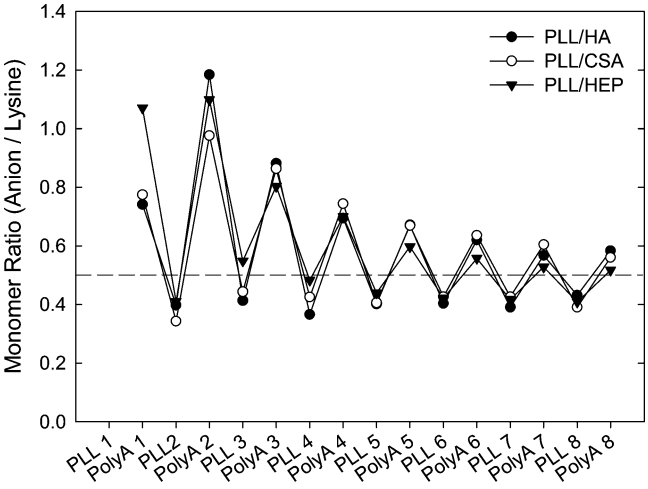

Figure 8. Evolution of the monomeric ratios of disaccharide monomer unit/lysine during the alternate deposition of PLL and polysaccharide layers for PLLHA (●), PLL/CSA (○), and PLL/HEP (▼). The ratio stabilizes toward a value of 0.5 (dotted line is plotted to guide the eyes).

the repeated patterns that govern PLL arrangement "around" the polyanion have roughly the same length scale in the three films. Of note, although HA, CSA, and HEP slightly differ in their MW, the similitude between the monomer ratios also suggest that MW of the polysaccharides is not playing an important role in the chemical composition and ionic pairing in the films.

A consequence of the invariance of the monomer ratio for the different anionic disaccharides is that the charge ratios in the films, calculated here by dividing the number of positive charges to that of negative charges, directly depend on the charge of the disaccharide monomers and decreases when the monomer charge is increased (Figure 9). As HA contains only one COO^- group, the PLL/HA films were found to be positively charged with a ratio of 1.67. PLL/CSA films with two charged groups per CSA were close to neutrality (ratio at 1.1), and finally, the PLL/HEP films exhibited the lowest ratio (0.46) as heparin bears 3.5 charges per monomer. Of note, the ratio was found to depend linearly on the disaccharide charge (inset in Figure 9).

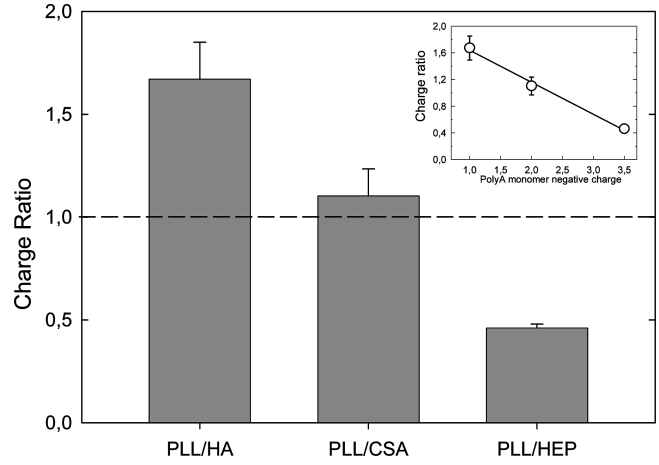

Figure 9. Charge ratio deduced from the quantitative analysis of the FTIR spectra for the three types of films. The charge ratio is the ratio of the number of positive charges over negative charges within the films. The doted line corresponding to a ratio of 1 (film with an entirely intrinsic charge matching if the groups are not sterically hindered) is plotted to guide the eyes. The error bars represent the standard deviation of two independent experiments. Inset: charge ratio as a function of the disaccharide monomeric charge (1 for PLL/HA, 2 for CSA, and 3.5 for HEP).

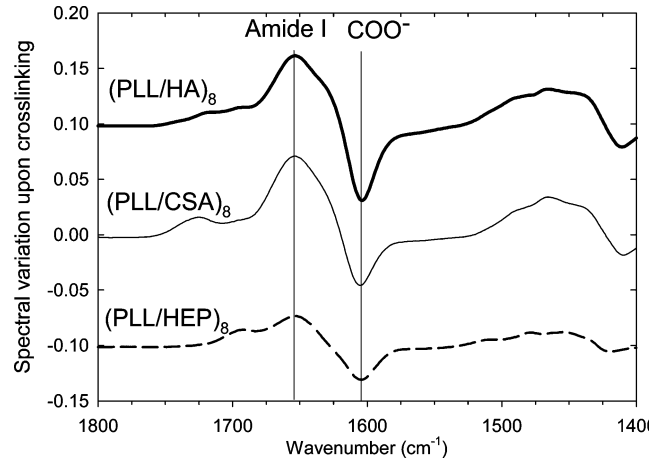

Figure 10. Differences in the FTIR spectra upon cross-linking measured for the three types of films (the difference corresponds to the subtraction of the spectrum of the $(PLL/PolyA)_8$ film to that of the film after cross-linking and final rinsing step). The spectra have been arbitrarily shifted for more clarity. The amide I band and COO- band are also indicated.

Ion Pairing. Thanks to the spectral separation of COO^- versus SO_3^- in the FTIR spectra and because COO^- groups close to NH_3^+ groups can be converted in covalent amide bonds by cross-linking, it is possible to quantify the respective amounts of NH_3^+ groups interacting with COO^- groups or with SO_3^- groups. This cross-linking reaction has been previously applied to films containing only COO^- groups as negative charges[50,59] and is employed here to selectively quantify the COO^- groups interacting with NH_3^+ groups. Variations in the infrared absorption spectra before and after cross-linking are shown for the three types of films in Figure 10. No change in the infrared absorbance of sulfate groups or saccharide ring was noticed, thus confirming that the reaction is specific to amine and carboxylic groups (data not shown). In all cases, a clear increase in the amide band (around 1635 cm^{-1}) and a decrease in the carboxylic peak (1610 cm^{-1}) are observed, although less pronounced for HEP containing films. In fact, the NH_3^+ groups in PLL/HEP films most probably interact preferentially with

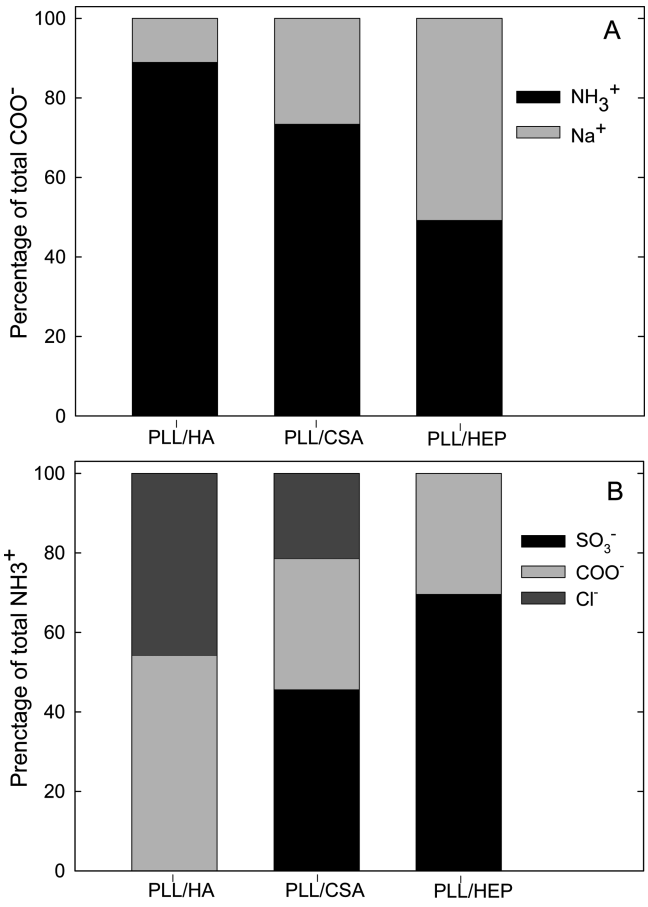

Figure 11. Ion pairing within the polysaccharide based films. From the quantitative analysis of the FTIR data, pairing of the carboxylic groups (A) and of the amine groups (B) was determined. For the COO^- groups, they can either be paired with an ammonium group or with a positive counterion (Na^+ in the case of NaCl). For the ammonium groups, they can be paired with a SO_3^- group, a COO^- group or a negative counterion (Cl^- in the case of NaCl).

the numerous sulfate groups (2.5 per disaccharide monomer) than with the single COO^- group, leaving some of these groups unpaired.

From the FTIR spectra of the cross-linking reactions, the percentage of COO^- groups involved in the cross-linking reaction was quantified (Figure 11A). It is assumed to be equal to the percentage of COO^- group paired in electrostatic interactions with NH_3^+ groups before cross-linking. This percentage was of 89% for (PLL/HA) films and of 74% for (PLL/CSA) films. In (PLL/HEP) films, only 49% were paired with NH_3^+ groups. The remaining COO^- groups are presumably involved in weaker interactions with the mobile Na^+ counterions due to the presence of 0.15 M NaCl in the rinsing solutions and because the charge neutrality in the film has to be respected. However, as Cl^- and Na^+ are not IR-active, it is not possible to get a direct proof of their presence. The presence of counterions is indeed strongly suggested by the effect of ionic strength on film growth and stability for films containing polysaccharides and polyaminoacids.[48,60] Few carboxylate groups may become protonated, but we verified that the percentage of protonated carboxylic groups was always below 7%. From these FITR data, ionic pairing could also be deduced for the ammonium groups. NH_3^+ groups are paired either with counterions ("free" groups), carboxylic groups, or sulfate groups for HEP and CSA-based films. One can first notice that the percentage of "free" NH_3^+ groups decreases when the sulfate content (and the overall negative charge) is increased. Thus, while 46% of the NH_3^+ groups in (PLL/HA) films are paired with counterions (or "free"), this percentage falls to 21% for PLL/CSA films and to almost zero for (PLL/HEP) films (Figure 11B), that is, all the NH_3^+ being engaged in electrostatic interactions and probably not highly mobile. These differences between the three polysaccharides may thus be related to the differences in the PLL diffusion coefficient measured by FRAP (Figure 7), that is, very few if no diffusion of PLL in HEP-based film, intermediate diffusion in CSA-based films and more diffusion in HA-based films. NH_3^+ groups interacting with COO- groups represent 54% of the total amines in (PLL/HA) films, and only 33% (respectively 30%) for both (PLL/CSA) (respectively (PLL/HEP)) films. Finally, the interaction between the NH_3^+ and SO_3^- groups accounts for 46% of total NH_3^+ in (PLL/CSA) films and 70% in (PLL/HEP) films.

The hypothesis that all SO_3^- groups are interacting with NH_3^+ (instead of having coexisting pairs of SO_3^-/Na^+ and NH_3^+/Cl^-) might lead to slightly overestimate the NH_3^+/SO_3^- ion pairing. Indeed, as it can be seen with COO^- in PLL/HA films, not all carboxylate groups are paired with NH_3^+. About 10% of the COO^- groups are interacting with counterions although an excess of NH_3^+/Cl^- is present, probably due to steric constraints. In a similar fashion, it is most probable that a fraction of the SO_3^- remain unpaired in the PLL/CSA and PLL/HEP films. In the case of HEP, as the average spacing between charges is 0.245 nm[61] is below the Bjerrum length (0.7 nm in our conditions), Manning condensation of the Na^+ counterions might be present.[62,63] However, such condensation, which is a consequence of strong electric field around the polyelectrolytes, only exists as the polyion is in dilute solution, particularly at low ionic strength and is no more present upon complexation with a polyelectrolyte of opposite charge.

Interestingly, one can notice that the proportions of the NH_3^+ groups interacting with COO^- versus SO_3^- groups are close to the molecules' stoechiometry. Indeed, in (PLL/CSA) which has a SO_3^- and a COO^-, 46% of the NH_3^+ groups interact with a SO_3^- group, and 33% with a COO^- group (close to the 1:1 ratio) and in PLL/HEP films, about 70% of the NH_3^+ interact with SO_3^- and 30% with COO^- (close to the 2.5:1 ratio). This would indicate that the "accessibility" of the negatively charged groups is very similar for all polysaccharides and that there does not seem to be any kind of specificity in the SO_3^- versus COO^- interactions with the ammonium groups.

Importance of Electrostatics, Hydrogen Bonds, and Water in the Interactions. All together, the results presented here show that significantly different behaviours are observed depending on the charge density and type of charge (COO^- versus SO_3^-) of the disaccharide monomer units. Interestingly, CSA, which has a double charge density than HA and a SO_3^- group, is closer to HA in its behavior than to HEP. Interactions of the different charged groups between them and with the surrounding water are probably responsible for these observations. In fact, water plays a key role in the structure of biological molecules like polysaccharides and polypeptides and accounts for their properties in solution. In particular, COO^- and SO_3^- are known to have different water affinities. As SO_3^- is larger than COO^-, it has a lower surface charge density because they have the same nominal net charge of -1. COO^- has a greater strength of interaction with the surrounding water and is considered as a kosmotrope.[32] Because the negative charge of SO_3^- is spread over three oxygens, it is a weakly hydrated anion and thus interacts strongly with weakly hydrated cations[51] such as the NH_3^+ group, which is usually considered as chaotrope.[52]

Due to the difference in their dehydration properties, the SO_3^-/ NH_3^+ interaction in water is stronger than the COO^-/ NH_3^+ interaction.[52]

The presence of the carboxylate groups in HA as well as CSA could, in part, explain why they form much more hydrated films than the highly sulfated HEP, the high hydration being associated with PLL diffusion. In HEP-based films, electrostatic interactions are expected to be stronger due to the presence of several sulfate groups and, as a consequence, no or very little diffusion is observed in these highly stitched films. The in vivo functions of HA and CSA are indeed directly related to their hydration properties,[64] whereas that of HEP is rather related to its interactions with proteins via its sulfate groups.[65] Although H-bonds are involved in the interactions between HEP and PLL,[66] they are probably less numerous than for CSA and HA.

Of note, HA and CSA have in common the presence of an acetamido group on the side chain that is absent in heparin. This acetamido group is indeed known to be involved in the formation of intramolecular hydrogen bonds connecting neighboring sugar units via the NH hydrogen of the acetamido group and the oxygen atoms of the COO- group.[67,68] Beside intramolecular H-bonds, it has been shown that water-mediated bonds are present in both CSA and HA. Molecular dynamics simulations give an estimate of 20 H-bonds per CSA disaccharide unit,[67] and in dried films of HA (i.e., that should in principle be "water free") the number of residual water molecules is still 4.5 per disaccharide unit.[69] Thus, interplay between electrostatic interactions between charged groups, hydrogen-bonds within and between saccharide units is at the origin of the properties of the polysaccharide-based films.

Conclusion

This work provides the first basis for the quantification of internal ion pairing in polysaccharide-based films (extrinsic versus intrinsic charges). Electrostatic interactions as well as water-mediated interactions (hydrogen bonds) are important in the film buildup. Important differences exist depending on film hydration and on the sulfate/carboxylate content of the films. Interestingly, although they differ in their charge, the disaccharide units equally "attract" approximately two lysine groups per monomer. As a consequence, the (±) charge ratio depends on the disaccharide net charge, and HA-based films are in large excess of positive charges that are neutralized by counterions. The percentage of free NH_3^+ in the films, which decreases when the charge density of the disaccharide increases, seems to be related to PLL diffusion and, as a consequence, directly influences film growth. Getting insight into glycosaminoglycan-based films contributes to a better understanding of the self-assembly processes occurring in vivo in natural extracellular matrices, including complex protein/GAG interactions via the positively charged lysine and arginine groups. This will also help for the design of tissue engineered constructs. Transport phenomena, in particular, diffusion of ions, proteins, and drugs, which are essential in vivo, could be mimicked and better understood using these biomimetic reservoirs having different hydration levels.

Acknowledgment. This work has been supported by the "Association Française contre les Myopathies" (AFM, Grant No. 12671), by the "Association pour la Recherche sur la Cancer" (equipment Grant No. 7918), by the "Fondation Recherche Médicale" (equipment Grant No. INE20061108297), and by "Agence Nationale pour la Recherche" (Grant ANR-06-NANO-006). C.P. is a Junior Member of the "Institut Universitaire de France", whose support is gratefully acknowledged. T.C. thanks the AFM for a Ph.D. fellowship. We are undebted to Bernard Senger (INSERM U595, Strasbourg) for his help in the FRAP data analysis and for Karine Glinel for careful reading of this manuscript.

Supporting Information Available. The calculation for the estimation of the diffusion coefficient from the FRAP is given. The calibration curves of the polyelectrolytes in solution (15 mg/mL) in contact with the ATR-FTIR crystal are also presented. Finally, the function $F(t/d_P) = 1 - \exp[-2(t/d_P)]$ is represented as a function of t/d_P with the corresponding linear fit. The inset shows the difference (expressed in %) between the linear fit and $F(t/d_P)$. This material is available free of charge via the Internet at http://pubs.acs.org.

References and Notes

(1) (a) Decher, G. *Science* **1997**, *277*, 1232–1237. (b) Ladam, G.; Schaad, P.; Voegel, J.-C.; Schaaf, P.; Decher, G.; Cuisinier, F. J. G. *Langmuir* **2000**, *16*, 1249–1255.
(2) Sukhishvili, S.; Granick, S. *Macromolecules* **2002**, *35*, 301–310.
(3) Picart, C.; Lavalle, P.; Hubert, P.; Cuisinier, F. J. G.; Decher, G.; Schaaf, P.; Voegel, J.-C. *Langmuir* **2001**, *17*, 7414–7424.
(4) (a) McAloney, R. A.; Sinyor, M.; Dudnik, V.; Goh, M. C. *Langmuir* **2001**, *17*, 6655–6663. (b) Lavalle, P.; Gergely, C.; Cuisinier, F.; Decher, G.; Schaaf, P.; Voegel, J.-C.; Picart, C. *Macromolecules* **2002**, *35*, 4458–4465.
(5) Picart, C.; Mutterer, J.; Richert, L.; Luo, Y.; Prestwich, G. D.; Schaaf, P.; Voegel, J.-C.; Lavalle, P. *Proc. Natl. Acad. Sci. U.S.A.* **2002**, *99*, 12531–12535.
(6) (a) Schlenoff, J.; Ly, H.; Li, M. *J. Am. Chem. Soc.* **1998**, *120*, 7626–7634. (b) Schlenoff, J. B.; Dubas, S. T. *Macromolecules* **2001**, *34*, 592–598.
(7) (a) Riegler, H.; Essler, F. *Langmuir* **2002**, *18*, 6694–6698. (b) Lourenco, J. M.; Ribeiro, P. A.; Botelho do Rego, A. M.; Braz Fernandes, F. M.; Moutinho, A. M.; Raposo, M. *Langmuir* **2004**, *20*, 8103–9. (c) Jaber, J. A.; Schlenoff, J. B. *Langmuir* **2007**, *23*, 896–901.
(8) Krzeminski, A.; Marudova, M.; Moffat, J.; Noel, T. R.; Parker, R.; Wellner, N.; Ring, S. G. *Biomacromolecules* **2006**, *7*, 498–506.
(9) (a) Tang, Z.; Wang, Y. l.; Podsiadlo, P.; Kotov, N. A. *Adv. Mater.* **2006**, *18*, 3203–3224. (b) Picart, C. *Curr. Med. Chem.* **2008**, 685–697.
(10) Nishinari, K.; Takahashi, R. *Curr. Opin. Colloid Interface Sci.* **2003**, *8*, 396–400.
(11) Schlessinger, J.; Lax, I.; Lemmon, M. *Cell* **1995**, *83*, 357–60.
(12) Taipale, J.; Keski-Oja, J. *FASEB J.* **1997**, *11*, 51–9.
(13) Wiig, H.; Gyenge, C.; Iversen, P. O.; Gullberg, D.; Tenstad, O. *Microcirculation* **2008**, *15*, 283–96.
(14) Drury, J. L.; Mooney, D. J. *Biomaterials* **2003**, *24*, 4337–51.
(15) Almond, A. *Cell. Mol. Life Sci.* **2007**, *64*, 1591–6.
(16) Ma, L.; Zhou, J.; Gao, C.; Shen, J. *J. Biomed. Mat. Res. B* **2007**, *83*, 285–292.
(17) Schneider, A.; Vodouhê, A.; Richert, L.; Francius, G.; Le Guen, E.; Schaaf, P.; Voegel, J.-C.; Frisch, F.; Picart, C. *Biomacromolecules* **2007**, *8*, 139–145.
(18) (a) Fujii, T.; Sun, Y. L.; An, K. N.; Luo, Z. P. *J. Biomech.* **2002**, *35*, 527–31. (b) Pavlov, G.; Finet, S.; Tatarenko, K.; Korneeva, E.; Ebel, C. *Eur. Biophys. J.* **2003**, *32*, 437–49. (c) Rodriguez-Carvajal, M. A.; Imberty, A.; Perez, S. *Biopolymers* **2003**, *69*, 15–28.
(19) Laurent, T. C. *The chemistry, biology, and medical applications of hyaluronan and its derivatives*; Cambridge University Press: Cambridge, U.K., 1998; Vol. 72.
(20) Machens, H. G.; Berger, A. C.; Mailaender, P. *Cells Tissues Organs* **2000**, *167*, 88–94.
(21) Tezcaner, A.; Hicks, D.; Boulmedais, F.; Sahel, J.; Schaaf, P.; Voegel, J. C.; Lavalle, P. *Biomacromolecules* **2006**, *7*, 86–94.
(22) (a) Ronca, F.; Palmieri, L.; Panicucci, P.; Ronca, G. *Osteoarthritis Cartilage* **1998**, *6*, 14–21. (b) Lamari, F. N. *Connect. Tissue Res.* **2008**, *49*, 289–92.
(23) Varki, A. *Essentials of glycobiology*; Cold Spring Harbor Laboratory Press: Cold Spring Harbor, New York, 1999.
(24) Kidane, A. G.; Salacinski, H.; Tiwari, A.; Bruckdorfer, K. R.; Seifalian, A. M. *Biomacromolecules* **2004**, *5*, 798–813.

(25) (a) Rider, C. C. *Biochem. Soc. Trans.* **2006**, *34*, 458–60. (b) Lonai, P. *Curr. Top. Dev. Biol.* **2005**, *66*, 37–64.
(26) Rezania, A.; Healy, K. E. *Biotechnol. Prog.* **1999**, *15*, 19–32.
(27) Kirker, K. R.; Luo, Y.; Nielson, J. H.; Shelby, J.; Prestwich, G. D. *Biomaterials* **2002**, *23*, 3661–71.
(28) Suh, J. K. F.; Matthew, H. W. T. *Biomaterials* **2000**, *21*, 2589–2598.
(29) Nettles, D. L.; Elder, S. H.; Gilbert, J. A. *Tissue Eng.* **2002**, *8*, 1009–1016.
(30) (a) Ishihara, M.; Obara, K.; Ishizuka, T.; Fujita, M.; Sato, M.; Masuoka, K.; Saito, Y.; Yura, H.; Matsui, T.; Hattori, H.; Kikuchi, M.; Kurita, A. *J. Biomed. Mater. Res.* **2003**, *64A*, 551–9. (b) Kumar, M. N. V. R. *React. Funct. Polym.* **2000**, *46*, 1–27.
(31) Kuettner, K. E.; Lindenbaum, A. *Science* **1964**, *144*, 1228–9.
(32) Asthagiri, D.; Schure, M. R.; Lenhoff, A. M. *J. Phys. Chem. B* **2000**, *104*, 8753–8761.
(33) Markarian, M. Z.; Moussallem, M. D.; Jomaa, H. W.; Schlenoff, J. B. *Biomacromolecules* **2007**, *8*, 59–64.
(34) Berg, J.; Tymoczko, J.; Stryer, L. *Biochemistry*. W. H. Freeman and Company: New York, 2002.
(35) Muller, M.; Brissova, M.; Rieser, T.; Powers, A. C.; Linkwitz, K. *Mater. Sci. Eng., C* **1999**, *8-9*, 163–169.
(36) Kuettner, K. E.; Lindenbaum, A. *Biochim. Biophys. Acta* **1965**, *101*, 223–5.
(37) (a) Höök, F.; Rodahl, M.; Brzezinski, P.; Kasemo, B. *J. Colloid Interface Sci.* **1998**, *208*, 63–67. (b) Rodahl, M.; Kasemo, B. *Rev. Sci. Instrum.* **1996**, *67*, 3238–3241.
(38) Sauerbrey, G. *Z. Phys.* **1959**, *155*, 206–222.
(39) Voinova, M. V.; Rodahl, M.; Jonson, M.; Kasemo, B. *Phys. Scr.* **1999**, *59*, 391–396.
(40) Schwinté, P.; Voegel, J.-C.; Picart, C.; Haikel, Y.; Schaaf, P.; Szalontai, B. *J. Phys. Chem. B* **2001**, *105*, 11906–11916.
(41) Richert, L.; Boulmedais, F.; Lavalle, P.; Mutterer, J.; Ferreux, E.; Decher, G.; Schaaf, P.; Voegel, J.-C.; Picart, C. *Biomacromolecules* **2004**, *5*, 284–294.
(42) Foot, M.; Mulholland, M. *J. Pharm. Biomed. Anal.* **2005**, *38*, 397–407.
(43) Sushko, N. I.; Firsov, S. P.; Zhbankov, R. G.; Tsarenkov, M.; Marchewka, M.; Ratajczak, C. *J. Vib. Spectrosc.* **1994**, *61*, 704–707.
(44) Boulmedais, F.; Bozonnet, M.; Schwinté, P.; Voegel, J.-C.; Schaaf, P. *Langmuir* **2003**, *19*, 9873–9882.
(45) Harrick, N. J. *J. Opt. Soc. Am.* **1965**, *55*, 851–859.
(46) Xie, A. F.; Granick, S. *Macromolecules* **2002**, *35*, 1805–1813.
(47) Harrick, N. J. *Internal reflection spectroscopy*; London, 1967.
(48) Richert, L.; Arntz, Y.; Schaaf, P.; Voegel, J.-C.; Picart, C. *Surf. Sci.* **2004**, *570*, 13–29.
(49) Boulmedais, F.; Tang, C. S.; Keller, B.; Voros, J. *Adv. Funct. Mater.* **2006**, *16*, 63–70.
(50) Schneider, A.; Francius, G.; Obeid, R.; Schwinté, P.; Frisch, B.; Schaaf, P.; Voegel, J.-C.; Senger, B.; Picart, C. *Langmuir* **2006**, *7*, 2882–2889.
(51) Collins, K. D. *Methods* **2004**, *34*, 300–11.
(52) Collins, K. D. *Biophys. Chem.* **2006**, *119*, 271–81.
(53) Picart, C.; Mutterer, J.; Arntz, Y.; Voegel, J. C.; Schaaf, P.; Senger, B. *Microsc. Res. Tech.* **2005**, *66*, 43–57.
(54) Wood, K. C.; Chuang, H. F.; Batten, R. D.; Lynn, D. M.; Hammond, P. T. *Proc. Natl. Acad. Sci. U.S.A.* **2006**, *103*, 10207–12.
(55) Voros, J. *Biophys. J.* **2004**, *87*, 553–61.
(56) Jourdainne, L.; Lecuyer, S.; Arntz, Y.; Picart, C.; Schaaf, P.; Senger, B.; Voegel, J. C.; Lavalle, P.; Charitat, T. *Langmuir* **2008**, *24*, 7842–7.
(57) Brant, D. A.; Flory, P. J. *J. Am. Chem. Soc.* **1965**, 87.
(58) Tanaka, K. *J. Biochem.* **1978**, *83*, 647–53.
(59) Picart, C.; Elkaim, R.; Richert, L.; Audoin, F.; Da Silva Cardoso, M.; Schaaf, P.; Voegel, J.-C.; Frisch, B. *Adv. Funct. Mater.* **2005**, *15*, 83–94.
(60) Richert, L.; Lavalle, P.; Payan, E.; Stoltz, J.-F.; Shu, X. Z.; Prestwich, G. D.; Schaaf, P.; Voegel, J.-C.; Picart, C. *Langmuir* **2004**, *1*, 284–294.
(61) Lerner, L.; Torchia, D. A. *J. Biol. Chem.* **1986**, *261*, 12706–14.
(62) Manning, G. S. *Q. Rev. Biophys.* **1978**, *11*, 179–246.
(63) Wang, J.; Rabenstein, D. L. *Biochemistry* **2006**, *45*, 15740–7.
(64) Laurent, T. C.; Laurent, U. B.; Fraser, J. R. *Ann. Rheum. Dis.* **1995**, *54*, 429–32.
(65) Kanyo, Z. F.; Christianson, D. W. *J. Biol. Chem.* **1991**, *266*, 4264–8.
(66) Grant, D.; Long, W. F.; Williamson, F. B. *Biochem. J.* **1991**, *277* (Pt 2), 569–71.
(67) Kaufmann, J.; Mohle, K.; Hofmann, H. J.; Arnold, K. *Carbohydr. Res.* **1999**, *318*, 1–9.
(68) Scott, J. E.; Heatley, F.; Hull, W. E. *Biochem. J.* **1984**, *220*, 197–205.
(69) Haxaire, K.; Marechal, Y.; Milas, M.; Rinaudo, M. *Biopolymers* **2003**, *72*, 149–61.

BM8012378